Integrated Morphological, Transcriptomic, and Metabolomic Profiling Reveals Differential Development Mechanisms in Two Weeping Forsythia Genotypes during Tissue Culture

Yanxia He
Henan University
Yanping Zheng
Henan University
Jiaqi Geng
Henan University
Xu Lu
Henan University
Xiaoxiao Wang
Henan University
Xin Sun
Henan University
Xiaoqian Zhang
Henan University
Xianping Wang
Henan University
Wangjun Yuan
10200068@vip.henu.edu.cn

Henan University https://orcid.org/0000-0002-8717-4649

Research Article

Keywords: Weeping forsythia, Tissue culture, Metabolomics, Transcriptome

Posted Date: June 17th, 2025

DOI: https://doi.org/10.21203/rs.3.rs-6833324/v1

Abstract

Weeping forsythia (*Forsythia suspensa*) is an important medicinal and ornamental plant. To explore genotype-dependent growth variation under tissue culture, we compared two long-style genotypes, FLS-1 and FLS-2. FLS-1 exhibited reduced plant height, branching, internode length, and chlorophyll content, along with chlorosis and impaired chloroplast ultrastructure. Transcriptomic analysis identified 2,059 and 3,482 DEGs between FLS-1 and FLS-2 on days 25 and 35, respectively, with 46 DEGs related to photosynthesis. Metabolomic profiling revealed 563 DEMs, with 15 KEGG pathways significantly enriched. These results elucidate key molecular differences affecting growth and photosynthesis between *F. suspensa* genotypes in vitro.

Key Message

Elucidating the molecular mechanisms underlying growth differences between *Forsythia* genotypes in tissue culture.

1. Introduction

Weeping forsythia (*Forsythia suspensa* (Thunb.) Vahl), a deciduous shrub belonging to the Oleaceae family, is renowned for its medicinal and ornamental value. The fruit of this species, commonly referred to as "Forsythiae Fructus" in Traditional C hinese Medicine (TCM), is extensively used for the treatment of various conditions, including gonorrhea, erysipelas, inflammation, pyrexia, and ulcers (Zhou et al. 2022; Liu et al. 2022). *F. suspensa* is naturally distributed across regions in China, such as Henan, Shanxi, Shaanxi, and Hebei (Gao et al. 2024). Its branches are characterized by their graceful, arching form, and the plant produces vibrant yellow flowers that bloom in early spring. These attributes make it a popular choice for urban greening and beautification initiatives (Li et al. 2021).

Given its medicinal, ornamental, and economic significance, *F. suspensa* has garnered increasing attention in recent years. However, the growing market demand and diminishing natural resources have underscored the importance of cultivation, presenting substantial opportunities for its development in rural areas (Li et al. 2024). Micropropagation, a tissue culture technique, enables the production of millions of clonal individuals through the induction of morphogenesis from various plant tissues or organs. This approach is widely utilized for the large-scale propagation of medicinal and ornamental plant species, as well as for the conservation of valuable genetic resources, including *Dendrobium* (Teixeira et al. 2015), *Saussurea involucrata* (Kuo et al. 2015), and *Cannabis sativa* (Adhikary et al. 2021). Consequently, plant tissue culture serves as a highly effective platform for the large-scale cultivation and production of superior forsythia germplasm. It ensures a consistent and sustainable supply of raw materials for TCM without exerting pressure on natural habitats (Niazian 2019; Zhang et al. 2023).

In the case of weeping forsythia, a comprehensive and efficient in vitro rapid propagation system has been successfully developed using tissue culture technology (Yuan et al. 2023). Notably, significant variations in growth and development have been observed among different weeping forsythia genotypes

under optimal culture conditions, highlighting the influence of genetic diversity on in vitro propagation outcomes.

In this study, an optimized tissue culture system was established for two distinct genotypes (FLS-1 and FLS-2) of weeping forsythia under laboratory conditions. Key growth indices, ultrastructural characteristics, and the chlorophyll a and chlorophyll b contents of subcultured seedlings were systematically evaluated. Comparative transcriptomic and metabolomic analyses were conducted to identify differentially expressed genes (DEGs) and differentially expressed metabolites (DEMs) between the two genotypes of FLS-1 and FLS-2. These findings provide valuable insights into the photosynthetic difference and underlying mechanisms driving growth differences among genotypes of weeping forsythia during tissue culture.

2. Materials and methods

2.1 Plant materials and samples

Two elite weeping forsythia genotypes, FLS-1 and FLS-2, were used as experimental materials. The plants were cultivated in the field at Da Mei Lian Qiao Company, Sanmenxia, Henan Province, China. Tissue culture experiments were conducted in the laboratory of the School of Life Sciences, Henan University. Healthy stem segments of FLS-1 and FLS-2 were selected as explants and inoculated onto an optimized and sterilized Murashige and Skoog (MS) medium supplemented with 3.0 $mg \cdot L^{-1}$ 6-benzylaminopurine (6-BA), 1.0 $mg \cdot L^{-1}$ indole-3-butyric acid (IBA), 30 $g \cdot L^{-1}$ sucrose, and 7 $g \cdot L^{-1}$ agar, adjusted to pH 6.0 prior to sterilization. The cultures were maintained under optimal conditions: a temperature of 25°C, a light intensity of 2,000–2,500 lx, and a photoperiod of 12 hours light and 12 hours darkness. Subsequently, the seedlings were subcultured under the same conditions.

2.2 Determination of growth index and chlorophyll content during the tissue culture of *F. suspensa*

Plant heights of FLS-1 and FLS-2 were measured every 5 days over 1-month period, beginning on the 10th day of subculture, with each measurement performed in triplicate. Fresh leaves were collected on the 25th and 35th day for chlorophyll determination. Chlorophyll was extracted using 80% acetone for 24 hours in darkness, and its content was quantified using a spectrophotometer following the method described as Mircea (Mircea et al. 2023).

2.3 Anatomical Structure Observation

The transmission electron microscopy (TEM) protocol was adapted from the method of Zhou et al. with minor modifications (Zhou et al. 2023). The middle region of the third leaf from 35-day-old subcultured seedlings was harvested for analysis. Leaf samples were immediately fixed in a solution containing 5% glutaraldehyde and 4% paraformaldehyde, buffered with 0.1 M sodium phosphate (pH 7.2). Following rinsing in the same buffer, the samples were post-fixed in 1% osmium tetroxide, also in 0.1 M sodium

phosphate (pH 7.2), for 3 hours at 4°C. The specimens were subsequently dehydrated through a graded ethanol series, transferred to acetone, and infiltrated with Epon812 epoxy resin for embedding. Ultra-thin sections were then prepared using a Leica EM UC7 ultramicrotome and stained with uranyl acetate and lead citrate. The prepared sections were examined using a FEI Talos F200C transmission electron microscope (Thermo Fisher Scientific, USA) for ultrastructural analysis.

2.4 RNA extraction, library construction and sequencing

The whole tissue culture seedlings of FLS-1 and FLS-2 were harvested on the 25th day and 35th day at noon, immediately flash-frozen in liquid nitrogen, and stored at -80°C for subsequent transcriptome sequencing analysis. Each group consisted of three biological replicates.Total RNA was extracted from tissue samples using TRIzol® Reagent according to the manufacturer's instructions. RNA quality was assessed using the 5,300 Bioanalyzer (Agilent) and quantified with the ND-2000 spectrophotometer (NanoDrop Technologies). Only high-quality RNA samples, meeting the criteria of OD260/280 = 1.8–2.2, OD260/230 ≥ 2.0, and a RNA Integrity Number (RIN) ≥ 6.5, were used for library construction.

RNA purification, library construction, and sequencing were performed by Shanghai Majorbio Bio-pharm Biotechnology Co., Ltd. (Shanghai, China). Raw sequencing data were processed for quality control and trimming using the fastp tool (https://github.com/OpenGene/fastp) (Chen et al. 2018), employing default parameters. Clean reads were then aligned to the reference genome in orientation mode using HISAT2 (http://ccb.jhu.edu/software/hisat2/index.shtml) (Kim et al. 2015;Li et al. 2023). The mapped reads for each sample were subsequently assembled as per the method outlined by Pertea et al (Pertea et al. 2015).

2.5 Differential expression analysis and functional enrichment

To identify DEGs between the two samples, transcript expression levels were quantified using the Fragments Per Kilobase of exon model per Million mapped fragments (FPKM) method. Gene abundances were calculated using RSEM (http://deweylab.github.io/RSEM/) (Li et al. 2011). Differential expression analysis was conducted with DESeq2 (http://bioconductor.org/packages/stats/bioc/DESeq2) (Love et al. 2014). Genes with an absolute $\log_2$ fold change ($|\log_2 FC|$) ≥ 2 and a false discovery rate (FDR) < 0.05 were considered significantly differentially expressed.

Gene Ontology (GO) (Ashburner et al. 2000) and Kyoto Encyclopedia of Genes and Genomes (KEGG) (Kanehisa and Goto 2000) enrichment analyses were performed to elucidate the functional roles and biological pathways associated with the DEGs.

2.6 qRTPCR validation

Primers for the 10 selected DEGs were designed using Primer 5.0 software (Lalitha 2000). Quantitative Real-time polymerase chain reaction (qRT-PCR) was performed using a LightCycler® 480 Real-Time PCR System (Roche, Switzerland) with the Hieff qPCR SYBR Green Master Mix (Yisheng, Shanghai, China).

The elongation factor-1α (EF-1α) gene served as an internal reference for normalization. Gene-specific primer sequences are provided in Table S1.

Relative gene expression levels were calculated using the method as Qi et al (Qi et al. 2019). Each experiment included three biological replicates and three technical replicates to ensure accuracy and reproducibility.

2.7 Metabolomics analyses

Samples of FLS-1 and FLS-2 were collected on the 35th day at noon of subculture for metabolomic analysis, with each group consisting of three biological replicates. The samples, along with grinding beads, were placed into centrifuge tubes for metabolite extraction. LC-MS/MS analysis was performed by Majorbio Bio-Pharm Technology Co., Ltd. (Shanghai, China) following standard protocols (Lu et al. 2008). Data analysis was conducted using the Majorbio Cloud Platform (https://cloud.majorbio.com) following database retrieval. Principal Component Analysis (PCA) and Orthogonal Partial Least Squares-Discriminant Analysis (OPLS-DA) were performed on the pre-processed data matrix using the ropls package (version 1.6.2) in R language. The model's stability and reliability were assessed through seven cycles of interactive cross-validation.

Differential metabolites between the two groups were mapped to biochemical pathways using metabolic enrichment and pathway analysis based on the KEGG database (http://www.genome.jp/kegg/) (Kanehisa et al. 2000). These metabolites were further classified according to their involvement in specific pathways or their functional roles.

3. Results

3.1 Growth of FLS-1 is significantly slower than FLS-2 during tissue culture

The proliferation and growth of weeping forsythia seedlings became noticeable after the 10th day of subculture. Compared to FLS-2, the growth of FLS-1 was significantly slower, as evidenced by a reduced average plant height and the appearance of chlorosis, characterized by distinctly lighter green leaves (Fig. 1). Furthermore, FLS-1 exhibited significantly fewer total nodes, branches, and a shorter average internode length compared to FLS-2 (Table 1). These findings indicate that the period from the 25th to the 35th day represents a phase of rapid growth in weeping forsythia under tissue culture conditions.

Table 1
Phenotypic data of FLS-1 and FLS-2 subcultured seedlings during growth

	Single Plant Height (mm)		Total Number of Branches(pcs)		Number of Branches (pcs)		Average Internode Length(mm)	
	FLS-1	FLS-2	FLS-1	FLS-2	FLS-1	FLS-2	FLS-1	FLS-2
10d	4.37 ± 0.25e	6.18 ± 0.28F	1.42 ± 0.12e	2.25 ± 0.11F	1.29 ± 0.09b	1.83 ± 0.08C	1.31 ± 0.13a	1.72 ± 0.09D
15d	4.87 ± 0.26e	8.96 ± 0.44F	1.54 ± 0.13e	3.08 ± 0.22E	1.38 ± 0.12ab	2.00 ± 0.10BC	1.34 ± 0.10a	1.76 ± 0.22D
20d	6.35 ± 0.4de	15.76 ± 0.64E	1.88 ± 0.19de	3.92 ± 0.19D	1.38 ± 0.12ab	2.00 ± 0.00BC	1.44 ± 0.10a	2.17 ± 0.16CD
25d	7.99 ± 0.59cd	20.05 ± 0.94D	2.54 ± 0.25cd	4.58 ± 0.23C	1.58 ± 0.12ab	2.04 ± 0.04BC	1.46 ± 0.16a	2.55 ± 0.19C
30d	9.18 ± 0.78bc	28.58 ± 1.37C	3.17 ± 0.27bc	5.96 ± 0.19B	1.63 ± 0.12ab	2.08 ± 0.06B	1.47 ± 0.17a	3.23 ± 0.23B
35d	10.66 ± 0.93b	40.1 ± 2.1B	3.63 ± 0.22ab	6.58 ± 0.22B	1.67 ± 0.12ab	2.08 ± 0.06B	1.50 ± 0.13a	4.89 ± 0.30A
40d	13.98 ± 1.24a	50.41 ± 2.54A	4.21 ± 0.39a	7.25 ± 0.35A	1.71 ± 0.14a	2.29 ± 0.09A	1.65 ± 0.18a	4.99 ± 0.31A

Note: Different lowercase letters and uppercase letters within the same column indicate the significant differences between FLS-1 and FLS-2 in different time points, respectively ($p < 0.05$).

3.2 Significant difference in chlorophyll content between the two genotypes

In this study, the chlorophyll a content of FLS-1 was 0.51 mg•g^{-1} on the 25th day, whereas FLS-2 exhibited a content of 1.41 mg•g^{-1}. On the 35th day, the chlorophyll a content was 0.60 mg•g^{-1} in FLS-1 and 1.10 mg•g^{-1} in FLS-2. For chlorophyll b, the content was 0.161 mg•g^{-1} in FLS-1 and 0.409 mg•g^{-1} in FLS-2 on the 25th day, and 0.190 mg•g^{-1} in FLS-1 and 0.363 mg•g^{-1} in FLS-2 on the 35th day. Statistical analysis using a T-test demonstrated significant differences in both chlorophyll a and chlorophyll b contents between FLS-1 and FLS-2 (Fig. 2).

3.3 Difference of leaf ultrastructure between two genotypes

At low magnification, the chloroplasts in mesophyll cells of FLS-1 and FLS-2 were in rings close to the cell wall. However, the palisade tissue cells of FLS-2 were small and neatly arranged, while that of FLS-1 were relatively large and loosely (Fig. 3a,b,e). The chloroplast morphology of FLS-2 was smooth, the bilayer membrane structure was complete and clear, and the structure of the inner capsule was clearly visible (Fig. 3d). Generally, 2–3 starch granules can be seen in a single chloroplast (Fig. 3c). While the morphological edge of FLS-1 was fuzzy, the boundary of the bilayer membrane was unclear, and the

texture of the inner capsule overlaps could not be identified. The number of starch granules in a single chloroplast was visibly reduced (Fig. 3g,h).

3.4 Transcriptome analysis

A total of 12 forsythia tissue culture seedling samples were sequenced using the Illumina NovaSeq 6,000 platform. After filtering out low-quality sequences, a total of 96.96 Gb of clean data were obtained. The effective data amount for each sample exceeded 6.04 Gb, with the average Q30 value of each sample being above 95.32%. The guanine-cytosine (GC) content ranged from 43.91–44.49%. Additionally, the overall alignment rate for the 12 samples ranged from 91.45–92.00%, with the unique mapping alignment rate ranging from 88.3–89.12% (Table 2).

Table 2
Quality control assessment of sequencing data

Sample	Clean reads	Q30(%)	GC content(%)	Total mapped	Uniquely mapped
25_FLS-1_1	55721004	95.54	44.08	51000271(91.53%)	49280832(88.44%)
25_FLS-1_2	59287946	95.63	44.24	54419881(91.79%)	52696039(88.88%)
25_FLS-1_3	59848444	95.68	44.05	54805232(91.57%)	53037157(88.62%)
25_FLS-2_1	57892392	95.58	44.26	52941403(91.45%)	51218413(88.47%)
25_FLS-2_2	40396634	95.32	44.27	36941403(91.45%)	35820138(88.67%)
25_FLS-2_3	59809034	95.66	44.21	54698240(91.45%)	52866257(88.39%)
35_FLS-1_1	62139654	95.59	44.06	56916878(91.6%)	54869701(88.3%)
35_FLS-1_2	63134870	95.72	44.00	57909494(91.72%)	55986672(88.68%)
35_FLS-1_3	54772656	95.66	43.91	50173731(91.6%)	48418411(88.4%)
35_FLS-2_1	48363582	95.61	44.13	44284768(91.57%)	42836722(88.57%)
35_FLS-2_2	49923374	95.51	44.21	45713008(91.57%)	44302334(88.74%)
35_FLS-2_3	47782580	95.57	44.49	43958249(92.0%)	42583282(89.12%)

Note: Sample: The name of the sample; Clean reads: The total number of items in the sequencing data after quality control; Q30 (%): Quality assessment of sequencing data after quality control, Q30 refer to the percentage of bases with sequencing quality above 99.9% in the total base; GC content (%): The percentage of the total sum of G and C bases corresponding to the quality control data in the total bases.

A total of 33,062 unigenes were annotated, and correlation analysis as well as PCA were performed for all samples. The PCA results showed that the expression patterns of FLS-1 and FLS-2 were distinctly separated, classifying them as independent groups (Fig. 4). Compared to FLS-2, a total of 2,059 DEGs were identified in FLS-1 on the 25th day, of which 1,078 were up-regulated and 981 down-regulated. On the 35th day, 3,482 DEGs were identified, with 2,059 up-regulated and 1,423 down-regulated (Fig. 5).

On the 25th day, up-regulated genes were primarily enriched in oxidoreductase activity, binding, secondary metabolic processes, and phenylpropanoid metabolism, while down-regulated genes were

mainly associated with photosynthesis and chlorophyll binding. On the 35th day, up-regulated genes were enriched in defense responses to external stimuli and oxidoreductase activity processes, while the down-regulated genes were again enriched in photosynthesis and chlorophyll binding, consistent with findings from the 25th day (Table S2).

On the 25th and 35th day, the DEGs of FLS-1 were mapped to 111 and 122 KEGG pathways, respectively, with 9 and 12 pathways significantly enriched. Notably, "photosynthesis" and "photosynthesis-antenna proteins" were among the significantly enriched pathways (Table 3). Based on GO and KEGG enrichment analyses, and considering the observed absence of chlorophyll in the FLS-1 samples, we focused on DEGs associated with the photosynthetic pathway. A total of 46 DEGs were identified, including 10 genes involved in photosystem I (PSI), 10 in photosystem II (PSII), 5 in F-type ATPase, 4 in the light-harvesting chlorophyll protein complex I (LHCI), and 13 in the light-harvesting chlorophyll protein complex II (LHCII). Notably, all of these genes showed down-regulated expression patterns, further indicating significant disruption of photosynthetic processes in FLS-1.

Table 3
KEGG pathway enrichment analysis of differentially expressed genes in FLS-1_vs_FLS-2 on the 25th and 35th day

Pathway ID	Description	Num	Pvalue	Qvalue
25d				
map00196	Photosynthesis-antenna proteins	10	1.00E-07	1.11E-05
map00052	Galactose metabolism	14	2.47E-04	9.14E-03
map00940	Phenylpropanoid biosynthesis	23	1.97E-04	1.09E-02
map00945	Stilbenoid, diarylheptanoid and gingerol biosynthesis	10	4.51E-04	1.25E-02
map00592	alpha-Linolenic acid metabolism	11	1.86E-03	2.96E-02
map04626	Plant-pathogen interaction	36	1.62E-03	2.99E-02
map00073	Cutin, suberine and wax biosynthesis	7	2.40E-03	3.33E-02
map00520	Amino sugar and nucleotide sugar metabolism	20	1.54E-03	3.41E-02
map00941	Flavonoid biosynthesis	9	2.84E-03	3.50E-02
35d				
map00196	Photosynthesis-antenna proteins	17	6.31E-14	7.70E-12
map00940	Phenylpropanoid biosynthesis	38	2.18E-06	1.33E-04
map04626	Plant-pathogen interaction	61	3.75E-05	1.52E-03
map00195	Photosynthesis	32	3.37E-04	5.87E-03
map00945	Stilbenoid, diarylheptanoid and gingerol biosynthesis	14	2.03E-04	6.20E-03
map00908	Zeatin biosynthesis	12	2.98E-04	7.28E-03
map00904	Diterpenoid biosynthesis	12	2.98E-04	7.28E-03
map00909	Sesquiterpenoid and triterpenoid biosynthesis	19	5.87E-04	8.95E-03
map00630	Glyoxylate and dicarboxylate metabolism	19	1.74E-03	2.36E-02
map00592	alpha-Linolenic acid metabolism	15	2.39E-03	2.91E-02
map04075	Plant hormone signal transduction	54	3.02E-03	3.35E-02

Note: Pathway id: The pathway identifier; Description: The name of the pathway; Num: The number of genes or transcripts enriched in this pathway; Pvalue: Uncorrected P-value, with smaller values indicating higher statistical significance; Qvalue: Adjusted p-value after correction.

Pathway ID	Description	Num	Pvalue	Qvalue
map00910	Nitrogen metabolism	11	3.85E-03	3.91E-02

Note: Pathway id: The pathway identifier; Description: The name of the pathway; Num: The number of genes or transcripts enriched in this pathway; Pvalue: Uncorrected P-value, with smaller values indicating higher statistical significance; Qvalue: Adjusted p-value after correction.

3.5 Metabolome profiles between FLS-1and FLS-2

To examine the differences in metabolites between tissue culture seedlings of two genotypes, metabolomics analysis was conducted using LC-MS. PCA was employed to analyze the metabolomic profiles and provide insights into distinct clustering patterns between the groups (Fig. 6). A total of 1,643 metabolites were identified, of which 1,595 had defined chemical formulas. The major classes of metabolites identified included terpenoids (16.18%), lipids (13.86%), carbohydrates and derivatives (9.53%), amino acids and derivatives (8.28%), and flavonoids (7.21%) (Fig. 7).

DEMs were identified using both univariate and multivariate analyses. In comparison to the FLS-2 genotype, 358 metabolites were upregulated and 205 were downregulated in FLS-1 samples. The 563 DEMs were mapped to 77 KEGG pathways, with 15 pathways showing significant enrichment. These included pathways such as arginine biosynthesis, β-alanine metabolism, flavonoid biosynthesis, diterpene biosynthesis, flavonoid and flavonol biosynthesis, and phenylpropanoid biosynthesis (Table 4).

Table 4
Significantly enriched pathways of differential metabolites

Pathway ID	Pathway Description	Num	Pvalue	Qvalue
map00590	Arachidonic acid metabolism	17	1.62E-10	1.25E-08
map00940	Phenylpropanoid biosynthesis	8	5.56E-04	2.14E-02
map00591	Linoleic acid metabolism	5	1.95E-03	5.01E-02
map01232	Nucleotide metabolism	7	2.73E-03	5.25E-02
map00380	Tryptophan metabolism	8	5.69E-03	8.77E-02
map00944	Flavone and flavonol biosynthesis	6	6.20E-03	7.95E-02
map00904	Diterpenoid biosynthesis	11	7.43E-03	8.17E-02
map00941	Flavonoid biosynthesis	7	1.05E-02	1.01E-01
map00460	Cyanoamino acid metabolism	5	1.55E-02	1.32E-01
map00770	Pantothenate and CoA biosynthesis	4	1.60E-02	1.23E-01
map00240	Pyrimidine metabolism	6	1.82E-02	1.27E-01
map00410	beta-Alanine metabolism	4	2.00E-02	1.28E-01
map00999	Biosynthesis of various plant secondary metabolites	9	2.71E-02	1.60E-01
map02010	ABC transporters	9	3.77E-02	2.08E-01
map00220	Arginine biosynthesis	3	3.85E-02	1.97E-01
map00470	D-Amino acid metabolism	6	6.55E-02	3.15E-01
map00780	Biotin metabolism	3	6.88E-02	3.12E-01
map00360	Phenylalanine metabolism	4	7.69E-02	3.29E-01
map00960	Tropane, piperidine and pyridine alkaloid biosynthesis	6	8.79E-02	3.56E-01
map00400	Phenylalanine, tyrosine and tryptophan biosynthesis	3	1.00E-01	3.86E-01

Note: Pathway id: The pathway identifier; Description: The name of the pathway; Num: The number of genes or transcripts enriched in this pathway; Pvalue: Uncorrected P-value, with smaller values indicating higher statistical significance; Qvalue: Adjusted p-value after correction..

3.6 Analysis of DEGs and DEMs in chlorophyll synthesis and plant hormone synthesis Pathway

Chlorophyll is a key pigment involved in the process of photosynthesis. KEGG pathway analysis identified a significant enrichment of 10 DEGs associated with chlorophyll synthesis. Further examination revealed that the expression of these genes was markedly downregulated at both the 25th and 35th days. Notably, the enzymes encoded by these downregulated genes encompass nearly the entire biosynthetic pathway of chlorophyll, including glutamyl-tRNA reductase (HemA), 5-aminolevulinic acid dehydratase (HemB), magnesium chelatase subunit H (chlH), magnesium protoporphyrin IX monomethyl ester (oxidative) cyclase (chlE), and protochlorophyllide reductase (por) (Fig. 8).

In this study, 13 DEGs involved in the gibberellin biosynthesis pathway were identified. These included 4 copalyl diphosphate synthase (CPS) genes, 1 ent-kaurene synthase (KS) gene, 1 kaurene oxidase (KO) gene, 2 ent-kaurenoic acid oxidase (KAO) genes, 1 GA20-oxidase (GA20ox) gene, 2 GA2-oxidase (GA2ox) genes, and 2 GA3-oxidase (GA3ox) genes. Expression analysis revealed that KS and KO genes were highly expressed on the 25th and 35th day, whereas CPS and GA20ox exhibited lower expression levels. Additionally, five DEMs involved in gibberellin biosynthesis were detected, including GA12-aldehyde, GA12, GA53, GA24, and GA7. Of these, the first four metabolites were upregulated, while GA7 was downregulated (Fig. 9a).

Further analysis identified 3 DEGs encoding S-adenosylmethionine synthetase (SAMS), 1 DEG encoding 1-aminocyclopropane-1-carboxylic acid synthase (ACS), and 1 DEG encoding 1-aminocyclopropane-1-carboxylic acid oxidase (ACO), all involved in ethylene biosynthesis. SAMS gene expression was significantly downregulated on both the 25th and 35th days, while ACS and ACO showed upregulation. In ethylene signal transduction, 17 DEGs were identified, including Constitutive Triple Response 1 (CTR1), EIN3-binding F-box 1/2 (EBF1/2), and Ethylene Response Factor 1 (ERF1), all of which were upregulated (Fig. 9b).

Three DEGs related to auxin biosynthesis were also identified, including 2 tryptophan decarboxylase (TDC) genes and 1 aldehyde dehydrogenase (ALDH) gene, with ALDH showing high expression at both time points. Furthermore, a total of 32 DEGs involved in auxin signal transduction were detected, consisting of 10 AUX/IAA genes, 3 Gretchen Hagen3 (GH3) genes, and 19 small auxin upregulated RNA (SAUR) genes. Notably, AUX/IAA and SAUR families were downregulated, while GH3 was upregulated (Fig. 9c).

Regarding cytokinin synthesis, 1 DEG encoding isopentenyl transferase (IPT) was downregulated, while 4 DEGs involved in cytokinin signal transduction were identified, including 2 cytokinin response 1 (CRE1) genes, 1 B-type Arabidopsis response regulator (B-ARR), and 1 A-type Arabidopsis response regulator (A-ARR). CRE1 was highly expressed, B-ARR was significantly downregulated, and A-ARR showed downregulation on day 25 and upregulation on day 35 (Fig. 9d).

Finally, 4 DEGs related to abscisic acid (ABA) biosynthesis were identified, including 1 lutein deficient 5 (LUT5) gene and 3 9-cis-epoxycarotenoid dioxygenase (NCED) genes, most of which showed low expression. In ABA signal transduction, 6 DEGs were identified, including 1 pyrabactin resistance 1-like (PYL) gene and 5 protein phosphatase 2C (PP2C) genes, with PYL highly expressed and PP2C genes

showing downregulation on day 25 and upregulation on day 35. Additionally, the expression of abscisic aldehyde (a DEM) was downregulated (Fig. 9e).

This comprehensive analysis highlights the intricate regulation of hormonal pathways, particularly gibberellin, ethylene, auxin, cytokinin, and ABA, in the development and signaling processes of tissue culture seedlings.

3.7 qRT-PCR validation

To validate the reliability of the transcriptome data, 10 DEGs, comprising 6 downregulated and 4 upregulated genes, were randomly selected from significantly enriched pathways for qRT-PCR analysis. The qRT-PCR results confirmed that the expression patterns of these genes were consistent with the RNA-Seq data, demonstrating the high reliability of the sequencing results for subsequent analyses (Fig. S1).

4 Discussion

Weeping forsythia is a widely distributed plant in China, valued for its ornamental, ecological, and medicinal properties (Li et al. 2023). To meet market demand and improve the quality of medicinal materials, artificial cultivation of forsythia has increased significantly in recent years (Yuan et al. 2023). Plant tissue culture technology has been employed to quickly generate superior varieties. Therefore, it is important to analyze the mechanism of causing the slow growth and development of some genotype (such as FLS-1) plants during tissue culture for weeping forsythia breeding.

Plant height is an important trait of plant phenotype, reflecting a certain stage of growth and development (Cheng et al. 2019). Studies have shown that plant dwarfing, lower ear height, and hindered growth and development are closely related to the decline of biological yield and economic yield (Hua 2009). In this study, compared to FLS-2, the seedlings of the FLS-1 genotype exhibited slower growth, pronounced leaf chlorosis, and a significant reduction in chlorophyll content. The chloroplast abnormalities of FLS-1 can be seen in the microstructure, such as blurred boundary of bilayer membrane, reduced internal starch granules, and unclear internal capsule stacking texture. These structural variations can seriously affect the light reaction in photosynthesis, resulting in lower photosynthetic efficiency of plants (Zhu et al. 2021; Kulkov et al. 2024; Wu et al. 2007). Chlorophyll is an important natural green pigment responsible for the absorption of light energy and conversion into chemical energy via photosynthesis in plants (da and Sant'Anna 2017). The complete biosynthetic pathway of chlorophyll, from glutamyl-tRNA to the production of chlorophyll a and chlorophyll b, involves approximately 20 distinct enzymatic steps. Protoporphyrin IX, a precursor to chlorophyll, is synthesized through several enzymatic steps (Nagata et al. 2005; Li et al. 2016). Mutations in the chlH gene have been shown to cause chlorophyll deficiency, resulting in a yellow or chlorotic phenotype in both *Oryza sativa* (Zhao et al. 2016) and *Arabidopsis thaliana* (Mochizuki et al. 2001). Kong et al (Kong et al. 2016) reported a novel rice mutant, YGL8, which displays a yellow-green leaf phenotype accompanied by abnormal chloroplast development. In the present study, transcriptome sequencing identified 10 DEGs associated with

chlorophyll biosynthesis, all of which showed down-regulated expression patterns. These genes include 2 HemA, 1 HemB, 2 chlH, 2 chlE, and 3 por (porphyrin biosynthetic enzymes). Glutamyl-tRNA reductase, a key enzyme in this pathway, is downregulated in FLS-1 compared to FLS-2. This may lead to reduced synthesis of 5-aminolevulinic acid (ALA) and protoporphyrin IX, impairing chlorophyll production and resulting in leaf color variation in the study (Fig. 8).

Hormonal homeostasis is pivotal in coordinating plant growth and development, with regulation occurring at multiple levels, including hormone biosynthesis, degradation, perception, and signal transduction (Zhang et al. 2023). Gibberellins (GAs), including GA1, GA3, GA4, and GA7, are diterpenoid hormones that regulate various aspects of plant growth and development, such as germination, stem elongation, flower formation, leaf senescence, and fruit ripening (Li et al. 2024; Lee et al. 2022; Wang et al. 2022). GAs are synthesized through complex pathways, with key enzymes like CPS, KS, KO, and KAO catalyzing the initial steps. Among the genes involved, GA20ox plays a critical role in regulating plant height (Elias et al. 2012). Inhibition of GA20ox reduces internode length and plant stature in apple trees, while its overexpression leads to increased height and branch diameter in pine trees (Park et al. 2015). Consistent with previous studies, our findings show that downregulation of GA20ox expression on day 25 and 35 resulted in reduced plant height and internode length in FLS-1. Metabolomics analysis revealed a decrease in GA7 levels. Attempts to promote FLS-1 growth by supplementing GA7 to MS medium, however, efforts to enhance FLS-1 growth by supplementing GA7 into MS medium yielded inconclusive results (Fig. 9a).

The biosynthesis of ethylene involves methionine conversion to S-adenosylmethionine (AdoMet) by SAMS, followed by its transformation to 1-aminocyclopropane-1-carboxylic acid (ACC) by ACS, and finally to ethylene by ACO (Van et al. 2014; Luo et al. 2018). ACS and ACO are critical enzymes in ethylene biosynthesis, maintaining balanced ethylene production during normal development (Khan et al. 2024).

Overexpression of CiACS4 induces a dwarf phenotype and increased ethylene release, while its suppression enhances plant height in transgenic citrus, demonstrating its key role in growth regulation (Chu et al. 2023). This is further supported by our findings, where the high expression of ACS and ACO enhances ethylene biosynthesis, thereby influencing the growth of FLS-1 and resulting in a dwarf phenotype (Fig. 9b). Auxin in plants can act directly on cell membranes and intracellular components to regulate essential processes such as cell division, elongation, and differentiation (Xing et al. 2024). The KEGG pathways enriched among the DEGs were auxin biosynthesis and signal transduction, suggesting that these two pathways are important to tissue culture seedling growth and development (Fig. 9c). In this study, the increased expression of the ALDH gene may lead to elevated auxin levels, subsequently suppressing the growth of FLS-1. Auxin-responsive genes, including the Auxin/Indole-3-Acetic Acid (AUX/IAA) family, auxin response factor (ARF) family, SAUR and the auxin-responsive GH3 family, play critical roles in regulating plant growth (Luo et al. 2018). Among these, the SAUR family contains the highest number of members. Recent research has demonstrated that SAUR genes primarily regulate plant cell elongation and cell wall relaxation (Lv et al. 2022; Luan et al. 2023). The observed inhibition of

FLS-1 tissue culture seedling growth in this study may be attributed to the downregulation of the SAUR homologous gene. The cytokinins (CKs) are known to regulate the biogenesis of chloroplasts, which are considered as one of the main groups of phytohormones as they, together with auxins, control cell division and, hence, influence the overall plant's architecture. The first step of CK biosynthesis is catalysed by IPT (Hluska et al. 2021). ABA is a key phytohormone regulating diverse physiological processes and influencing plant growth and development by modulating the production of protective metabolites (Singh et al. 2023). Key ABA biosynthetic genes, including zeaxanthin epoxidase (ZEP), NCED and abscisic aldehyde oxidase (AAO3), have been identified, with NCED-catalyzed xanthoxin production recognized as the primary regulatory step in ABA biosynthesis (Ng et al. 2014). ABA receptors, mainly comprising the PYR/PYL/RCAR protein family, undergo conformational changes upon binding ABA, forming receptor complexes that relieve PP2C-mediated inhibition of SnRK2, thereby activating SnRK2 through phosphorylation and initiating downstream ABA-responsive gene expression (Varshney et al. 2021). In this study, changes in the expression levels of the ABA biosynthetic gene NCED, receptor gene PYL, and signaling negative regulator gene PP2C suggest their potential involvement in the growth of *Forsythia suspensa* tissue culture seedlings. Metabolomic analysis further identified an upregulation of abscisic aldehyde, an ABA precursor, indicating enhanced ABA biosynthesis (Fig. 9e). Additionally, the downregulation of PP2C likely reduces its inhibitory effect on SnRK2, impairing SnRK2 phosphorylation and subsequently disrupting ABA signaling. Collectively, these findings suggest that altered ABA biosynthesis and signaling pathways may contribute to the growth inhibition observed in FLS-1 lines.

Abbreviations

AdoMet	S-adenosylmethionine
AAO3	Abscisic aldehyde oxidase
A-ARR	A-type arabidopsis response regulator
ABA	Abscisic acid
ACC	1-aminocyclopropane-1-carboxylic acid
ACO	1-aminocyclopropane-1-carboxylic acid oxidase
ACS	1-aminocyclopropane-1-carboxylic acid synthase
ALA	5-aminolevulinic acid
ALDH	Aldehyde dehydrogenase
ARF	Auxin response factor
ARF	Auxin response factor
AUX/IAA	Auxin/Indole-3-Acetic Acid
B-ARR	B-type arabidopsis response regulator
CKs	Cytokinins
CPS	Copalyl diphosphate synthase
CRE1	Cytokinin response 1
CTR1	Constitutive Triple Response 1
DEGs	Differentially expressed genes
DEMs	Differentially expressed metabolites
EBF1/2	EIN3-binding F-box 1/2
EF-1α	Elongation Factor-1α
ERF1	Ethylene Response Factor 1
FDA	False Discovery Rate
FPKM	Fragments Per Kilobase of exon model per Million mapped fragments
FLS	*Forsythia suspensa* withlong style
GAs	Gibberellins
GC	Guanine-Cytosine
GH3	Gretchen Hagen3
GO	Gene Ontology

IBA	Indole-3-butyric Acid
IPT	Isopentenyl transferase
KAO	Kaurenoic acid oxidase
KEGG	Kyoto Encyclopedia of Genes and Genomes
KO	Kaurene oxidase
KS	Kaurene synthase
LHCI	Light-harvesting chlorophyll protein complex I
LHCII	Light-harvesting chlorophyll protein complex II
LUT5	Lutein deficient 5
NCED	9-cis-epoxycarotenoid dioxygenase
OPLS-DA	Orthogonal Partial Least Squares-Discriminant Analysis
PCA	Principal Component Analysis
PP2C	Protein phosphatase 2C
PSI	Photosystem I
PSII	Photosystem II
PYL	Pyrabactin resistance 1-like
qRT-PCR	Quantitative Real-time polymerase chain reaction
RIN	RNA Integrity Number
SAMS	S-adenosylmethionine Synthetase
SAUR	Small auxin upregulated RNA
TCM	Traditional Chinese Medicine
TDC	Tryptophan decarboxylase
TEM	Transmission Electron Microscopy
ZEP	Zeaxanthin epoxidase
6-BA	6-benzylaminopurine

Declarations

Funding

This work was supported in part by grants from the Henan Science and Technology Research Project (252102110153) and the National Key Research and Development Program of China Project (2023YFD2201100).

Competing interests

The authors declare no competing interests.

Authors' contributions

YWJ, HYX. and WXP. conceived the research project.ZYP, GJQ, LX, WXX, SX and ZXQ. were involved in the analysis of the data. ZYP. drafted the paper and HYX. revised it critically for intellectual content. All authors have read and approved the final manuscript. All authors agree to be accountable for all aspects of the work.

Ethical Approval and Consent to participate

Not applicable. No human or animal subjects were involved in this research.

Consent for publication

All authors consent to the publication of this manuscript in its current form

Availability of supporting data

The sequence data that support the findings of this study are openly available in GenBank of NCBI at https://www.ncbi.nlm.nih.gov/, and the associated *SRA* numbers of the raw sequence data are from SRR27452189 to SRR27452200.

References

1. Ashburner M, Ball CA, Blake JA, Botstein D, Butler H, Cherry JM et al (2000) Gene ontology: tool for the unification of biology. The Gene Ontology Consortium. Nat Genet 25(1):25–29. https://doi.org/10.1038/75556
2. Adhikary D, Kulkarni M, El-Mezawy A, Mobini S, Elhiti M, Gjuric R et al (2021) Medical Cannabis and Industrial Hemp Tissue Culture: Present Status and Future Potential. Front Plant Sci 12:627240. https://doi.org/10.3389/fpls.2021.627240
3. Cheng Q, Dong LD, Su T, Li TY, Gan ZR, Nan HY et al (2019))CRISPR/Cas9-mediated targeted mutagenesis of GmLHY genes alters plant height and internode length in soybean. BMC Plant Biol 19(1):562. https://doi.org/10.1186/s12870-019-2145-8
4. Chu LL, Yan Z, Sheng XX, Liu HQ, Wang QY, Zeng RF et al (2023) Citrus ACC synthase CiACS4 regulates plant height by inhibiting gibberellin biosynthesis. Plant Physiol 192(3):1947–1968. https://doi.org/10.1093/plphys/kiad159

5. Chen SF, Zhou YQ, Chen YR, Gu J (2018) fastp: an ultra-fast all-in-one FASTQ preprocessor. Bioinformatics 34(17):i884–i890. https://doi.org/10.1093/bioinformatics/bty560
6. da Silva Ferreirada V, Sant'Anna C (2017) Impact of culture conditions on the chlorophyll content of microalgae for biotechnological applications. World J Microbiol Biotechnol 33(1):20. https://doi.org/10.1007/s11274-016-2181-6
7. Elias AA, Busov VB, Kosola KR, Ma C, Etherington E, Shevchenko O et al (2012) Green revolution trees: semidwarfism transgenes modify gibberellins, promote root growth, enhance morphological diversity, and reduce competitiveness in hybrid poplar. Plant Physiol 160(2):1130–1144. https://doi.org/10.1104/pp.112.200741
8. Gao BY, Zhu HS, Liu ZH, He XH, Sun JH, LI YF et al (2024) Chemical Compositions of Lianqiao (Forsythia suspensa) Extracts and Their Potential Health Benefits. Pharmaceuticals (Basel) 7(6):740. https://doi.org/10.3390/ph17060740
9. Hua Q (2009) Effect of water stress on maize yield during different growing stages (in Chinese). J Maize Sci 17(2):60–63. https://api.semanticscholar.org/CorpusID:111875327
10. Hluska T, Hlusková L, Emery RJN (2021) The Hulks and the Deadpools of the Cytokinin Universe: A Dual Strategy for Cytokinin Production, Translocation, and Signal Transduction. Biomolecules 11(2):209. https://doi.org/10.3390/biom11020209
11. Kulkov L, Arkhipov R, Abramova A, Vereshchagin M, Voronkov A, Khalilova V et al (2024) Long-term effects of silver nanoparticles and mineral nutrition components on the photosynthetic processes, chloroplast ultrastructure and productivity of Solanum lycopersicum plants. J Photochem Photobiol B 260:113038. https://doi.org/10.1016/j.jphotobiol.2024.113038
12. Kuo CL, Agrawal DC, Chang HC, Chiu YT, Huang CP, Chen YL et al (2015) In vitro culture and production of syringin and rutin in Saussurea involucrata (Kar. et Kir.) - an endangered medicinal plant. Bot Stud 56(1):12. https://doi.org/10.1186/s40529-015-0092-8
13. Khan S, Alvi AF, Saify S, Iqbal N, Khan NA (2024) The Ethylene Biosynthetic Enzymes, 1-Aminocyclopropane-1-Carboxylate (ACC) Synthase (ACS) and ACC Oxidase (ACO): The Less Explored Players in Abiotic Stress Tolerance. Biomolecules 14(1):90. https://doi.org/10.3390/biom14010090
14. Kanehisa M, Goto S (2000) KEGG: kyoto encyclopedia of genes and genomes. Nucleic Acids Res 28(1):27–30. https://doi.org/10.1093/nar/28.1.27
15. Kim D, Langmead B, Salzberg SL (2015) HISAT: a fast spliced aligner with low memory requirements. Nat Methods 12(4):357–360. https://doi.org/10.1038/nmeth.3317
16. Kong WY, Yu XW, Chen HY, Liu LL, Xiao YJ, Wang YL et al (2016) The catalytic subunit of magnesium-protoporphyrin IX monomethyl ester cyclase forms a chloroplast complex to regulate chlorophyll biosynthesis in rice. Plant Mol Biol 92(1–2):177–191. https://doi.org/10.1007/s11103-016-0513-4
17. Lalitha S (2000) Primer Premier 5. Biotech Softw Internet Rep 1(6):270–272. https://doi.org/10.1089/152791600459894

18. Lu WY, Bennett BD, Rabinowitz JD (2008) Analytical strategies for LC-MS-based targeted metabolomics. J Chromatogr B Analyt Technol Biomed Life Sci 871(2):236–242. https://doi.org/10.1016/j.jchromb.2008.04.031
19. Li B, Dewey CN (2011) RSEM: accurate transcript quantification from RNA-Seq data with or without a reference genome. BMC Bioinformatics 12:323. https://doi.org/10.1186/1471-2105-12-323
20. Love MI, Huber W, Anders S (2014) Moderated estimation of fold change and dispersion for RNA-seq data with DESeq2. Genome Biol 15(12):550. https://doi.org/10.1186/s13059-014-0550-8
21. Lv WZ, He X, Guo HJ, Lan HB, Jiao YQ, Li L et al (2022) Genome-Wide Identification of TaSAUR Gene Family Members in Hexaploid Wheat and Functional Characterization of TaSAUR66-5B in Improving Nitrogen Use Efficiency. Int J Mol Sci 23(14):7574. https://doi.org/10.3390/ijms23147574
22. Li Y, Shi LC, Pei NC, Cushman SA, Si YT (2021) Transcriptomic responses to drought stress among natural populations provide insights into local adaptation of weeping forsythia. BMC Plant Biol 21(1):273. https://doi.org/10.1186/s12870-021-03075-6
23. Liu LD, Sun Y, Wen CX, Jiang T, Tian W, Xie XL et al (2022) Metabolome analysis of genus forsythia related constituents in Forsythia suspensa leaves and fruits using UPLC-ESI-QQQ-MS/MS technique. PLoS ONE 17(6):e0269915. https://doi.org/10.1371/journal.pone.0269915
24. Li W, Tang S, Zhang S, Shan JG, Tang CJ, Chen QN et al (2016) Gene mapping and functional analysis of the novel leaf color gene SiYGL1 in foxtail millet [Setaria italica (L.) P. Beauv]. Physiol Plant 157(1):24–37. https://doi.org/10.1111/ppl.12405
25. Li Y, Wang F, Pei NC, Li Q, Liu HL, Yuan WJ et al (2023) The updated weeping forsythia genome reveals the genomic basis for the evolution and the forsythin and forsythoside A biosynthesis. Hortic Plant J 9(6):1149–1161. https://www.sciopen.com/article/ 10.1016/j.hpj.2022.09.004
26. Li QX, Xue XD (2024) Study on Synergistic Mechanism Between Forsythia Cultivation and Rural Development. J Life Sci Agric 1:68–72. https://doi.org/10.62517/jlsa.202407212
27. Luan J, Xin M, Qin ZW (2023) Genome-Wide Identification and Functional Analysis of the Roles of SAUR Gene Family Members in the Promotion of Cucumber Root Expansion. Int J Mol Sci 24(6):5940. https://doi.org/10.3390/ijms24065940
28. Lee BD, Yim Y, Cañibano E, Kim SH, García-León M, Rubio V et al (2022) CONSTITUTIVE PHOTOMORPHOGENIC 1 promotes seed germination by destabilizing RGA-LIKE 2 in Arabidopsis. Plant Physiol 189(3):1662–1676. https://doi.org/10.1093/plphys/kiac060
29. Li Y, Zhao LM, Guo CM, Tang M, Lian WL, Chen SY et al (2024) OsNAC103, an NAC transcription factor negatively regulates plant height in rice. Planta 259(2):35. https://doi.org/10.1007/s00425-023-04309-7
30. Luo J, Zhou JJ, Zhang JZ (2018) Aux/IAA Gene Family in Plants: Molecular Structure, Regulation, and Function. Int J Mol Sci 19(1):259. https://doi.org/10.3390/ijms19010259
31. Mochizuki N, Brusslan JA, Larkin R, Nagatani A, Chory J (2001) Arabidopsis genomes uncoupled 5 (GUN5) mutant reveals the involvement of Mg-chelatase H subunit in plastid-to-nucleus signal transduction. Proc Natl Acad Sci U S A 98(4):2053–2058. https://doi.org/10.1073/pnas.98.4.2053

32. Mircea DM, Calone R, Shakya R, Zuzunaga-Rosas J, Sestras RE, Boscaiu M et al (2023) Evaluation of Drought Responses in Two Tropaeolum Species Used in Landscaping through Morphological and Biochemical Markers. Life 13(4):960. https://doi.org/10.3390/life13040960
33. Niazian M (2019) Application of genetics and biotechnology for improving medicinal plants. Planta 249(4):953–973. https://doi.org/10.1007/s00425-019-03099-1
34. Ng LM, Melcher K, Teh BT, Xu HE (2014) Abscisic acid perception and signaling: structural mechanisms and applications. Acta Pharmacol Sin 35(5):567–584. https://doi.org/10.1038/aps.2014.5
35. Nagata N, Tanaka R, Satoh S, Tanaka A (2005) Identification of a vinyl reductase gene for chlorophyll synthesis in Arabidopsis thaliana and implications for the evolution of Prochlorococcus species. Plant Cell 17(1):233–240. https://doi.org/10.1105/tpc.104.027276
36. Park EJ, Lee WY, Kurepin LV, Zhang RC, Janzen L, Pharis RP (2015) Plant hormone-assisted early family selection in Pinus densiflora via a retrospective approach. Tree Physiol 35(1):86–94. https://doi.org/10.1093/treephys/tpu102
37. Pertea M, Pertea GM, Antonescu CM, Chang TC, Mendell JT, Salzberg SL (2015) StringTie enables improved reconstruction of a transcriptome from RNA-seq reads. Nat Biotechnol 33(3):290–295. https://doi.org/10.1038/nbt.3122
38. Qi XP, Ogden EL, Die JV, Ehlenfeldt MK, Polashock JJ, Darwish O et al (2019) Transcriptome analysis identifies genes related to the waxy coating on blueberry fruit in two northern-adapted rabbiteye breeding populations. BMC Plant Biol 19(1):460. https://doi.org/10.1186/s12870-019-2073-7
39. Singh A, Roychoudhury A (2023) Abscisic acid in plants under abiotic stress: crosstalk with major phytohormones. Plant Cell Rep 42(6):961–974. https://doi.org/10.1007/s00299-023-03013-w
40. Teixeira da Silva JA, Cardoso JC, Dobránszki J, Zeng SJ (2015) Dendrobium micropropagation: a review. Plant Cell Rep 34(5):671–704. https://doi.org/10.1007/s00299-015-1754-4
41. Varshney V, Majee M (2021) JA Shakes Hands with ABA to Delay Seed Germination. Trends Plant Sci 26(8):764–766. https://doi.org/10.1016/j.tplants.2021.05.002
42. Van de Poel B, Van Der Straeten D (2014) 1-aminocyclopropane-1-carboxylic acid (ACC) in plants: more than just the precursor of ethylene! Front Plant Sci 5:640. https://doi.org/10.3389/fpls.2014.00640
43. Wang YD, Huang X, Huang XM, Su W, Hao YW, Liu HC et al (2022) BcSOC1 Promotes Bolting and Stem Elongation in Flowering Chinese Cabbage. Int J Mol Sci 23(7):3459. https://doi.org/10.3390/ijms23073459
44. Wu ZM, Zhang X, He B, Diao LP, Sheng SL, Wang JL et al (2007) A chlorophyll-deficient rice mutant with impaired chlorophyllide esterification in chlorophyll biosynthesis. Plant Physiol 145(1):29–40. https://doi.org/10.1104/pp.107.100321
45. Xing N, Li XQ, Wu SH, Wang ZW (2024) Transcriptome and Metabolome Reveal Key Genes from the Plant Hormone Signal Transduction Pathway Regulating Plant Height and Leaf Size in Capsicum baccatum. Cells 13(10):827. https://doi.org/10.3390/cells13100827

46. Yuan WJ, He ZY, Zhang SP, Zheng YP, Zhang XQ, He SQ et al (2023) Comparative transcriptomics provides insights into the pathogenic immune response of brown leaf spots in weeping forsythia. Tree Physiol 43(9):1641–1652. https://doi.org/10.1093/treephys/tpad060
47. Zhang YQ, Berman A, Shani E (2023) Plant Hormone Transport and Localization: Signaling Molecules on the Move. Annu Rev Plant Biol 74:453–479. https://doi.org/10.1146/annurev-arplant-070722-015329
48. Zhu JC, Cai DF, Wang JP, Cao JH, Wen YC, He JP et al (2021) Physiological and anatomical changes in two rapeseed (Brassica napus L.) genotypes under drought stress conditions. Oil Crop Sci 6(02):97–104. https://doi.org/10.1016/j.ocsci.2016-0153
49. Zhou MY, Huo JH, Wang CR, Wang WM (2022) UPLC/Q-TOF MS Screening and Identification of Antibacterial Compounds in Forsythia suspensa (Thunb.) Vahl Leaves. Front Pharmacol 12:704260. https://doi.org/10.3389/fphar.2021.704260
50. Zhao SL, Long WH, Wang YH, Liu LL, Wang YL, Niu M et al (2016) rice White-stripe leaf3 (wsl3) mutant lacking an HD domain-containing protein affects chlorophyll biosynthesis and chloroplast development. J Plant Biol 59:282–292. https://doi.org/10.1007/s12374-016-0459-8
51. Zhang CC, Wang S, Wang YF, Wang HY, Qin M, Dai XY et al (2023) plication of tissue culture technology of medicinal plants in sustainable development of Chinese medicinal resources. Zhongguo Zhong Yao Za Zhi 48(5):1186–1193. https://doi.org/10.19540/j.cnki.cjcmm.20221017.104
52. Zhou YS, Zhang T, Wang XC, Wu WQ, Xing JJ, Li ZL et al (2023) A maize epimerase modulates cell wall synthesis and glycosylation during stomatal morphogenesis. Nat Commun 14(1):4384. https://doi.org/10.1038/s41467-023-40013-6

Figures

Figure 1

Growth status of FLS-1 and FLS-2 subcultured seedlings at different time periods

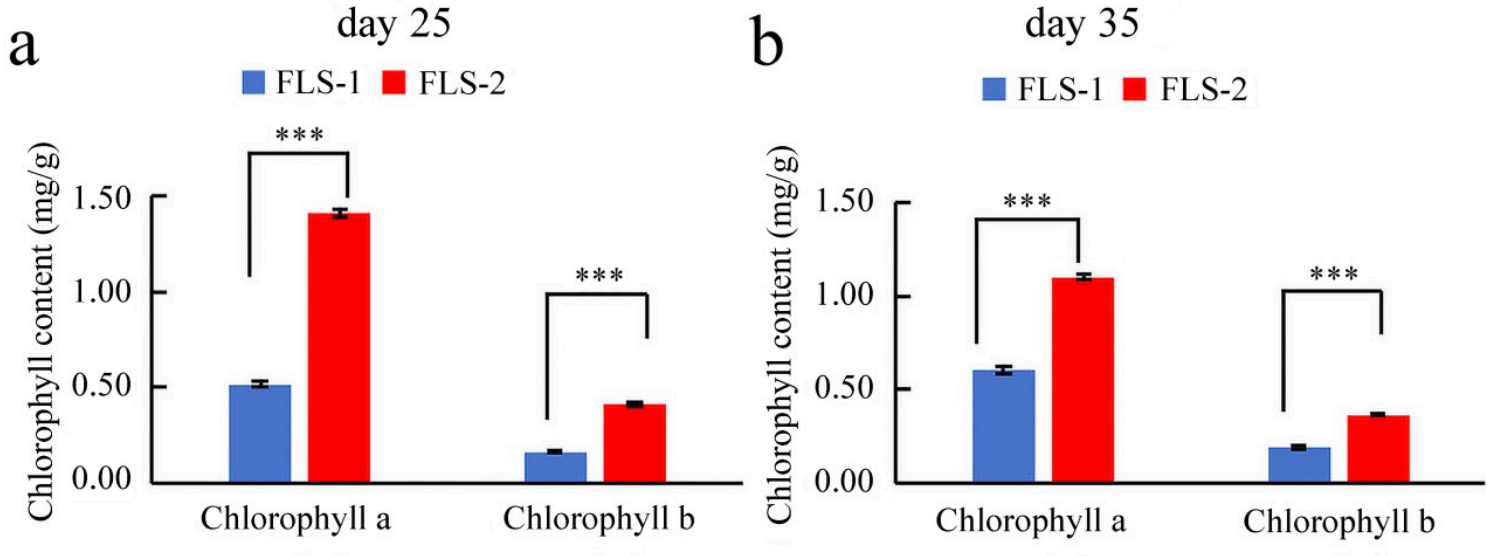

Figure 2

Chlorophyll content of FLS-1 and FLS-2 subcultured seedlings

Note: a and b refer chlorophyll content of FLS-1 and FLS-2 subcultured seedlings on the 25th day 35th day respectively. (***$p < 0.001$).

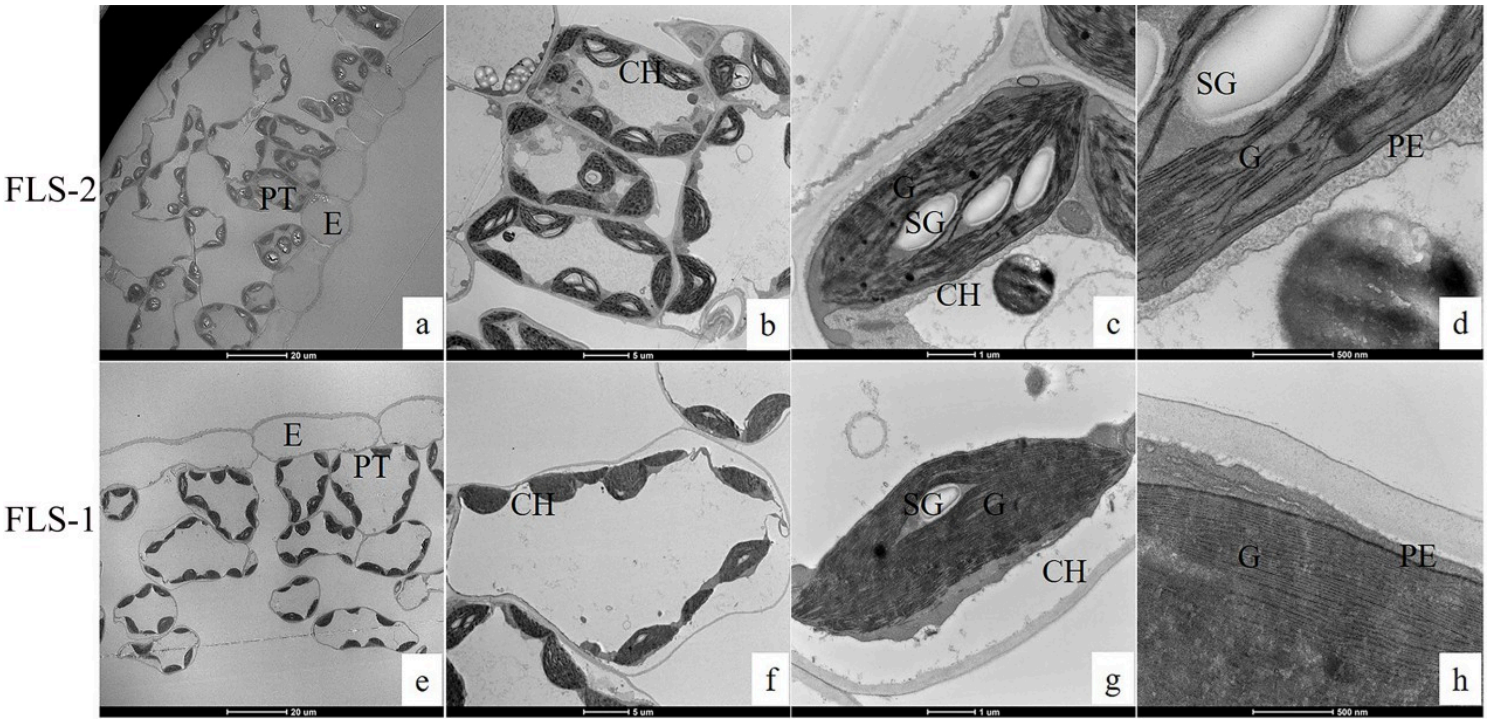

Figure 3

Ultrastructural differences in chloroplasts between two genotypes

Note: The images of chloroplast a-d for FLS-2 and e-h for FLS-1. Ch, chloroplast; CM, chloroplast membrane; E, epidermis cell tissue; PT, palisade mesophyll tissue; Sg, starch grain; G, granum.

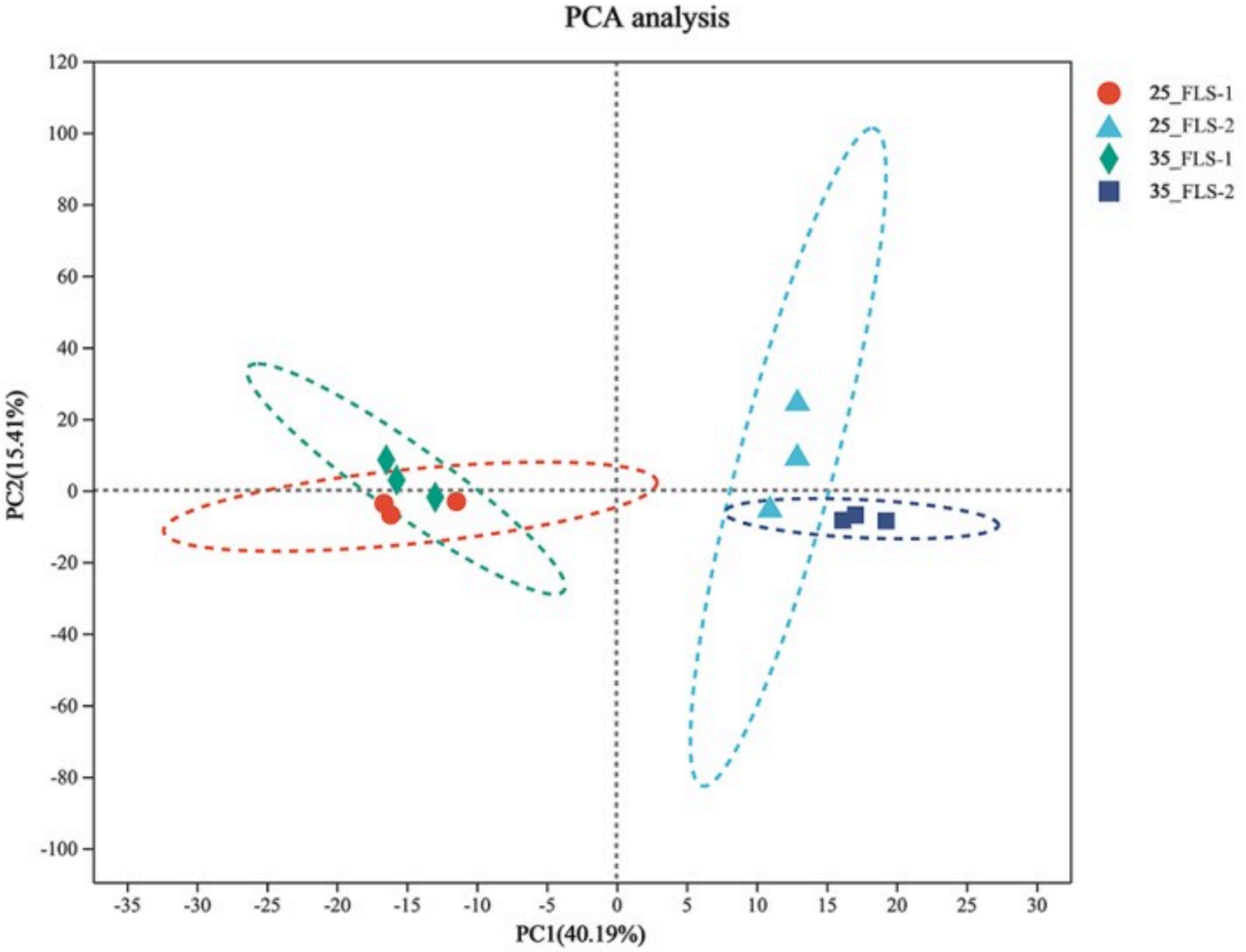

Figure 4

Principal component analysis (PCA) of the expression patterns

Note: The horizontal axis represents the contribution degree of principal component 1 (PC1) in the two-dimensional figure to the distinguished samples, and the vertical axis represents the contribution degree of principal component 2 (PC2) in the two-dimensional figure to the distinguished samples. The red circle indicates the 3 replicates of 25_FLS-1, the light blue triangle represents the 3 replicates of 25_FLS-2, the green diamond represents the 3 replicates of 35_FLS-1, and the dark blue square represents the 3 replicates of 35_FLS-2.

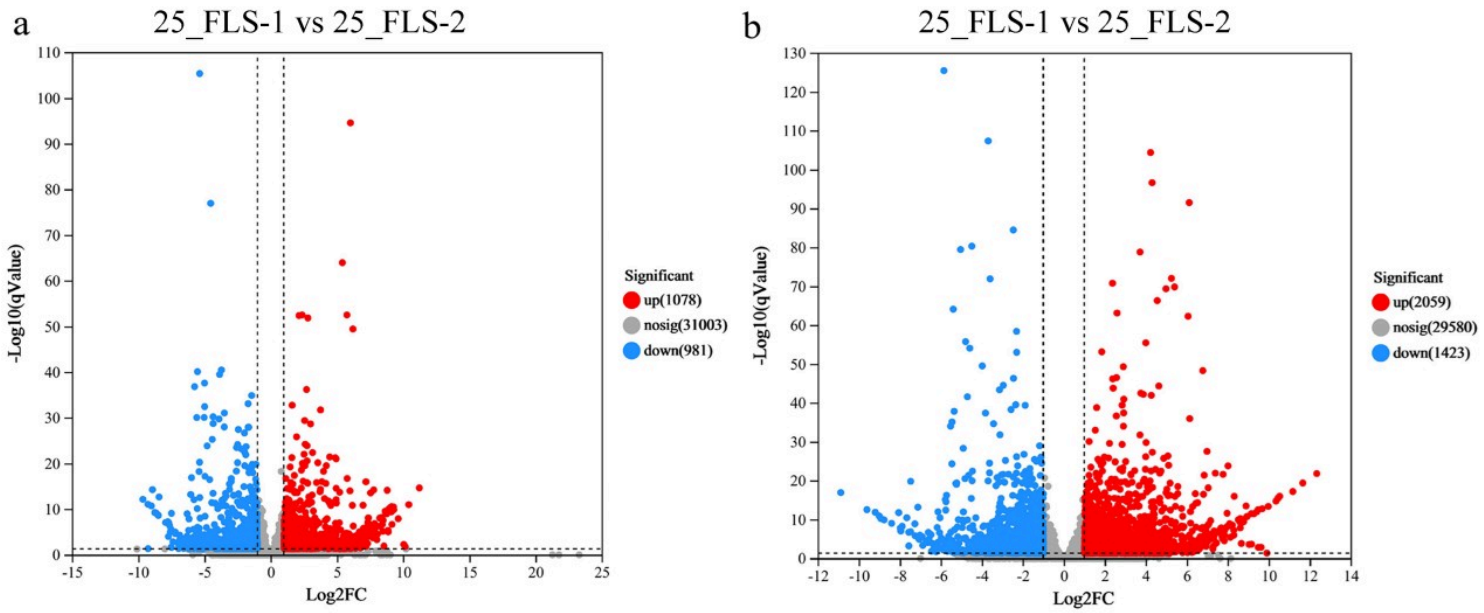

Figure 5

Volcano plots showing the number of DEGs between two genotype

Note: a and b refer Volcano plot analysis of differential genes on the 25th and 35th day, respectively. The horizontal axis represents the fold-change of gene expression between the two samples, and the vertical axis represents the statistical test value of gene expression difference. Red dots represent significantly up-regulated genes, blue dots represent significantly down-regulated genes, and gray dots represent non-significantly differenced genes. The closer the points are to the boundary, the more significant the expression difference.

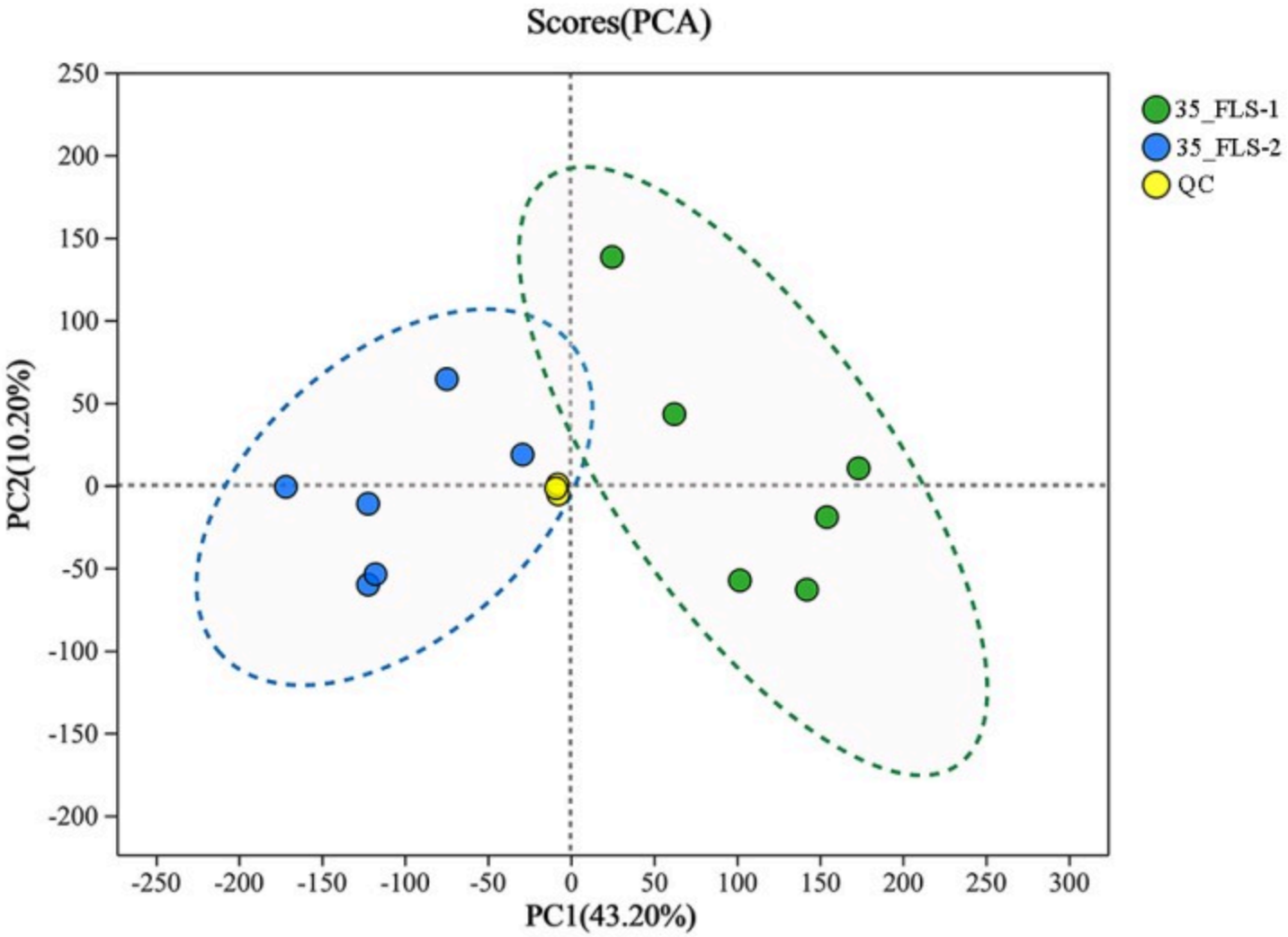

Figure 6

Principal component analysis (PCA) of metabolites for FLS-1 and FLS-2 samples

Note: The abscissa represents the first principal component, and the ordinate represents the second principal component; The green circle represents 6 replicate samples of 35_FLS-1, the blue circle represents 6 replicate samples of 35_FLS-2, and the yellow circle represents 3 replicate samples of quality control. QC: Quality control sample.

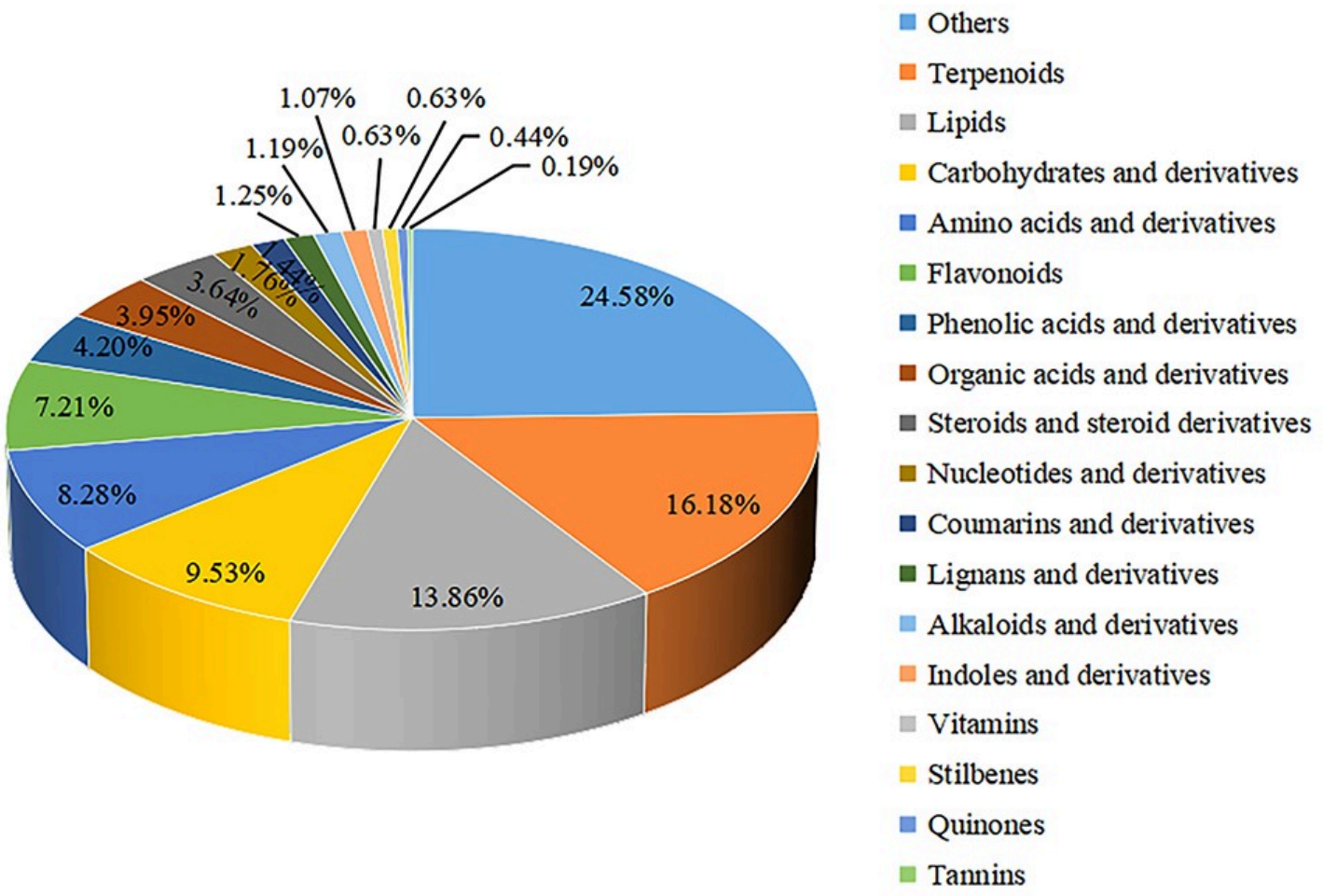

Figure 7

Annotation infographic of all metabolites

Note: Each color represents a different class of compounds

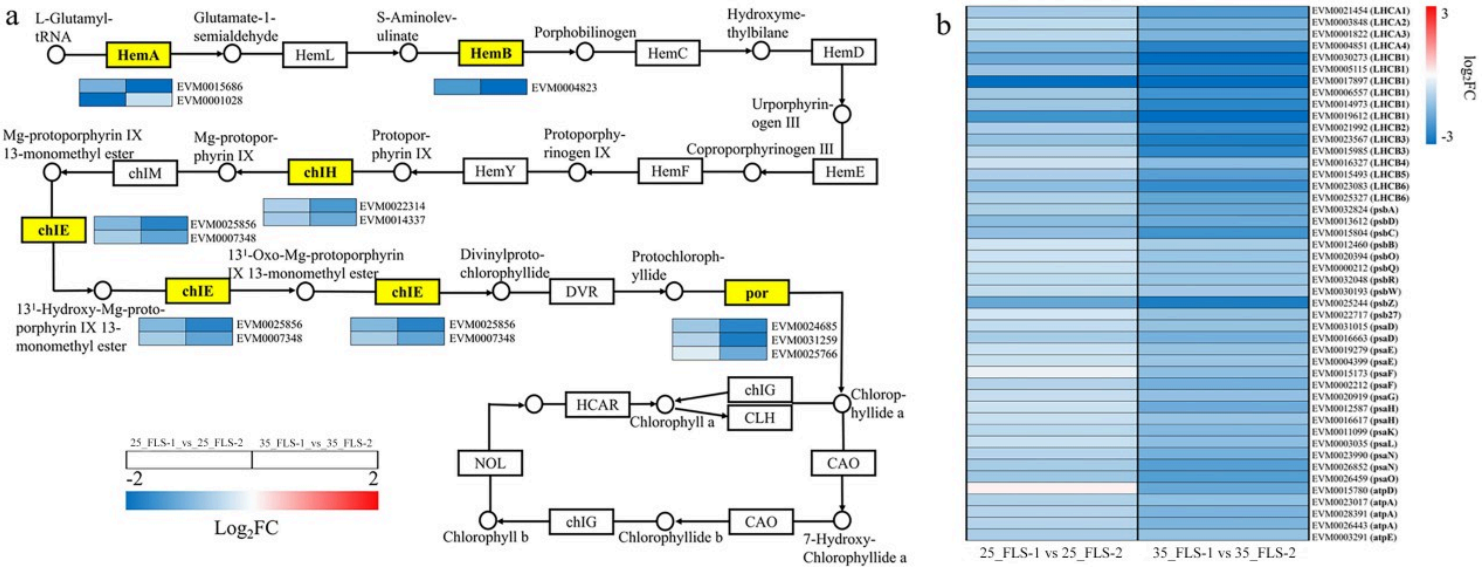

Figure 8

Differentially expressed genes (DEGs) in the chlorophyll metabolic pathway

Note: In the figure, circle represent chemical compounds, the blue oval box represent the synthetic related hormones, and the yellow box indicate the differentially expressed genes within each pathway. The EVM number corresponds to the gene ID. The two squares in the heatmap from left to right represent 25_FLS-1_vs_25_FLS-2 and 35_FLS-1_vs_35_FLS-2, The black text at the top of the heatmap represents the abbreviation of the enzyme name. Blue indicates down-regulation and red indicates up-regulation, the darker the color, the greater the fold change.

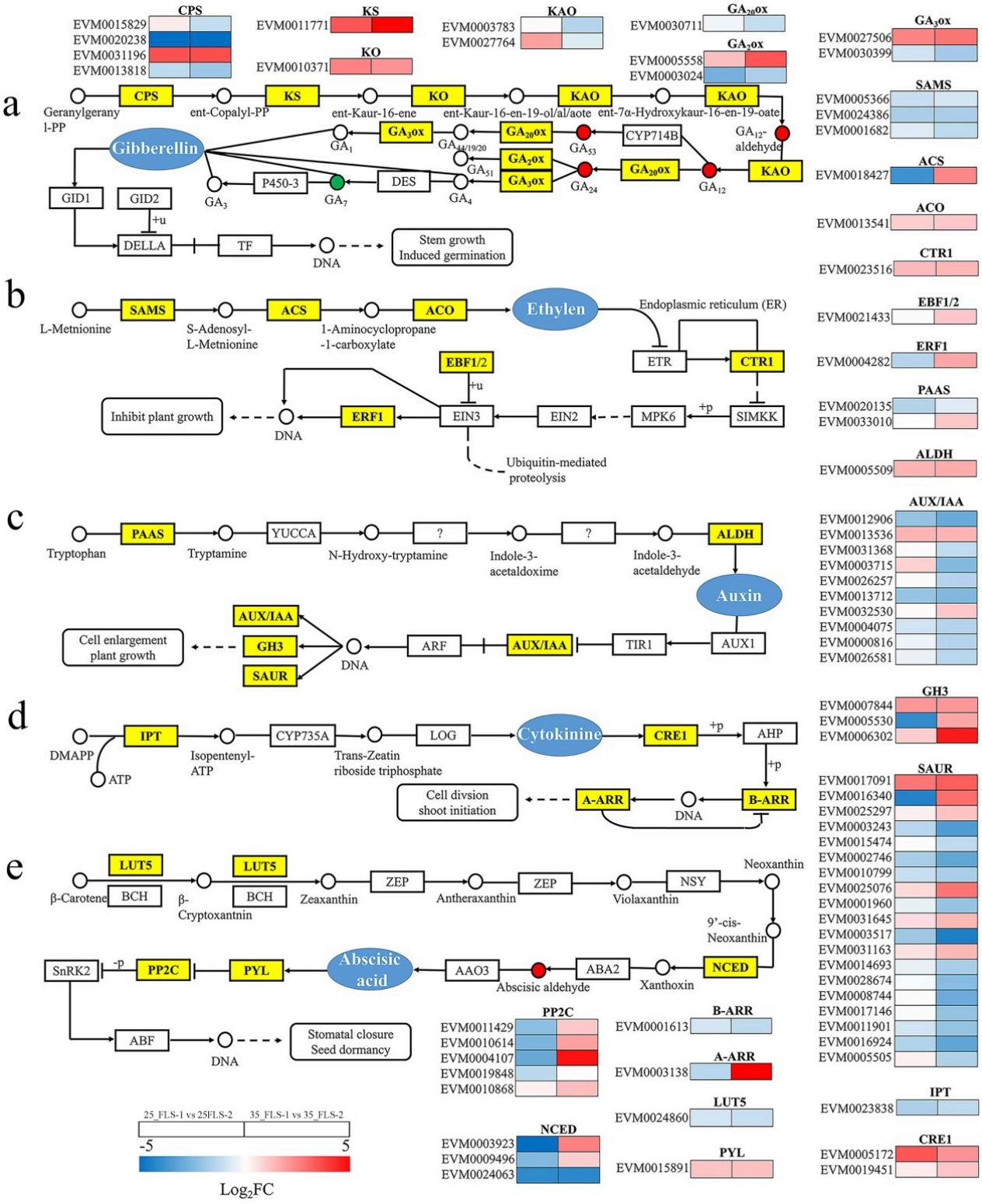

Figure 9

Differentially expressed genes (DEGs) in plant hormone biosynthesis pathways

Note: a-e refer Gibberellin, Ethylene, Auxin, Cytokinin and Abscisic acid respectively. In the figure, circle represent chemical compounds, the blue oval box represent the synthetic related hormones, and the yellow box indicate the differentially expressed genes within each pathway. The EVM number

corresponds to the gene ID. The two squares in the heatmap from left to right represent 25_FLS-1_vs_25_FLS-2 and 35_FLS-1_vs_35_FLS-2, The black text at the top of the heatmap represents the abbreviation of the enzyme name. Blue indicates down-regulation and red indicates up-regulation, the darker the color, the greater the fold change.

Supplementary Files

This is a list of supplementary files associated with this preprint. Click to download.

- 2025.6.6Additionalfile.docx